WILEY

An investigation into sky temperature estimation, its variation, and significance in heat transfer calculations of solar cookers

Ashish Karn [ORCID] | Venkateshwarlu Chintala | Suresh Kumar

Department of Mechanical Engineering, School of Engineering, University of Petroleum and Energy Studies (UPES), Energy Acres, Bidholi, Dehradun, Uttarakhand, India

Correspondence
Ashish Karn, Department of Mechanical Engineering, School of Engineering, University of Petroleum and Energy Studies, Dehradun, Uttarakhand 248007, India.
Email: akarn@ddn.upes.ac.in

Abstract

The determination of sky temperature assumes great importance in engineering applications such as radiative cooling of buildings. Many studies that involve a radiative exchange with the sky employ different reported models of sky temperature interchangeably. However, until now, hardly any systematic study has been done to quantify the errors/variations that might be encountered in calculating this radiative exchange employing these different correlations. In the current paper, first, a thorough analysis has been presented on the sky temperature correlations and a possible range of variation in sky temperature based on the estimation of sky emissivity is computed. Both diurnal-nocturnal variation in sky temperature and seasonal disparities in sky temperature have been reported. Next, the case of a box-type solar cooker has been taken up for investiga-

Nomenclature: ε, sky temperature emissivity; T_{sky}, sky temperature; T_a, ambient temperature; F_1, first-figure-of-merit for solar cookers; η_o, optical efficiency; U_L, overall coefficient of heat loss; T_p, plate temperature; θ_p, nondimensional plate temperature; U_t, top heat transfer factor; U_b, bottom heat transfer factor; U_s, side heat transfer factor; Q_t'', rate of heat loss per unit area from absorber plate to inner glass cover; h_{cpg1}, convective heat transfer coefficient from plate to first glass cover; h_{cg1g2}, convective heat transfer coefficient between two glass covers; h_w, convective heat transfer coefficient on the top of glass cover; ε_g, emissivity of glass; T_{g1}, outward temperature of first glass cover; P_v, vapor pressure of water; T_{dp}, dew-point temperature; RH, relative humidity (in percentage); $\varnothing$, relative humidity (in fraction); H_s, solar insolation; $RMSE$, root-mean-square error; $MAPE$, mean-absolute-percentage error; η_{ob}, optical efficiency for the beam component of irradiance; η_{od}, optical efficiency for the diffuse component of irradiance; Nu, Nusselt number; Ra, Raleigh number; h_{rpg1}, radiative heat transfer coefficient from plate to first glass cover; h_{rg1g2}, radiative heat transfer coefficient between two glass covers; h_{rg2s}, radiative heat transfer coefficient from glass cover to surrounding; ε_p, emissivity of plate; T_{g2}, outward temperature of second glass cover.

tion with respect to the possible influence of the sky temperature estimation in predicting its performance parameter, *first-figure-of-merit* on a daily, seasonal, and climatic basis. Our observations show an enormous difference in sky temperature depending upon the expressions of emissivity from which it is derived. The variability of sky temperature has a nominal influence on the prediction of *first-figure-of-merit*, although a marked discrepancy is observed across the seasons at the same location.

1 | INTRODUCTION

The sky longwave radiation exchange is an important component of radiative balance, relevant for multifarious thermal engineering applications such as the design of radiant cooling systems for buildings[1] and is primarily determined by the effective sky temperature.[2] The accurate knowledge of the radiative and other heat transfer characteristics of surfaces can prove fruitful in assessing the potential for radiative cooling of buildings that can stay cool without requiring any mechanical devices as well as in predicting the radiative losses from the solar collector covers and exposed surfaces of buildings.[1] Radiative cooling is a consequence of heat loss by longwave radiation emission toward the sky, where the sky can be treated as a heat sink for exterior surfaces of the buildings. Thus, due to its continuous energy exchange with the earth's surface, the sky can be considered to act as a global blackbody. Then, corresponding to this blackbody, a fictitious but useful terminology named as equivalent sky temperature can be defined, which is useful for practical calculations of heat exchange between any given surface at ground level and the sky. This equivalent sky temperature is mainly a function of the atmospheric temperature change with height near the earth's surface and the vertical distribution of water vapor in the atmosphere.[3,4] Clouds trap heat and tend to increase the sky temperature.[5] Although the sky temperature can be measured with instruments such as a pyrradiometer or a pyrgeometer, but these instruments are quite delicate, expensive, and the frequently required calibrations are sensitive to be carried out before measurements. Thus, the sky atmospheric temperature may alternatively be estimated using Stefan-Boltzmann law and the effective atmospheric emissivity.[6-8] Many models and empirical correlations have been proposed for estimating the effective sky emissivity, beginning with the seminal work by Ångström.[9] However, there exists inadequate concurrence between equivalent sky temperatures calculated by these differently proposed correlations. Each of these correlations is only acceptable in certain weather conditions or for a specific site. Moreover, even the same correlation can predict drastically different values of sky emissivity across different seasons or diurnal/nocturnal conditions. It is unclear as to how the errors in determining the atmospheric radiation can lead to erroneous predictions in different applications.

Thus, in the current work, the primary objective is to explore the effect of the variability caused by the estimation of sky temperature. Further, a typical case of a box-type solar cooker is being explored. In a solar collector or cooker, the top radiative heat losses to the atmosphere dictate its performance, and although many detailed reviews have focused on the box-type solar cookers,[10-16] it is still unclear as to how the errors in determining the effective sky temperature can lead to an erroneous prediction of the solar cooker performance. Thus, we explore the variability in the predicted performance of a solar cooker by employing different reported expressions of sky emissivity. Thus, using the meteorological measurements and suitable expressions for different parameters, the variation in sky temperature has been analyzed and the fluctuation in solar cooker performance has been evaluated. The solar cooker performance in the current study has been primarily evaluated by computing the first-figure-of-merit (referred hereafter as F_1) and according to the prior literature, F_1 gives a criterion to ensure that the stagnation temperature of solar cookers are sufficient to facilitate boiling type of cooking.[17] In the current paper, we restrict our attention upon the performance evaluation of solar cookers using the first factor of merit and its fluctuation due to sky temperature estimation. Moreover, we also explore the daily, seasonal, and climatic variations of the first-figure-of-merit of solar cookers in the Indian subcontinent. This paper is structured as follows: Section 2 provides the details of the methodology, including meteorological measurements and the experimental setup. Subsequently, in Section 3, we present an analysis of the estimation of sky temperature and the different underlying factors such as water vapor pressure and the dew-point temperature. Section 4 focuses on the effect of sky temperature in solar cooker performance prediction, followed by a final conclusion in Section 5.

2 | EXPERIMENTAL SETUP AND METHODOLOGY

2.1 | Measurements on solar cookers

Figure 1 presents a schematic of the box-type solar cooker used in the present study. Temperatures at different points in the solar cooker are measured with the help of calibrated Chromel-Alumel thermocouples (type K). Precalibrated thermocouples are attached to the center of the absorber plate, inner and outer glass surface of both glass
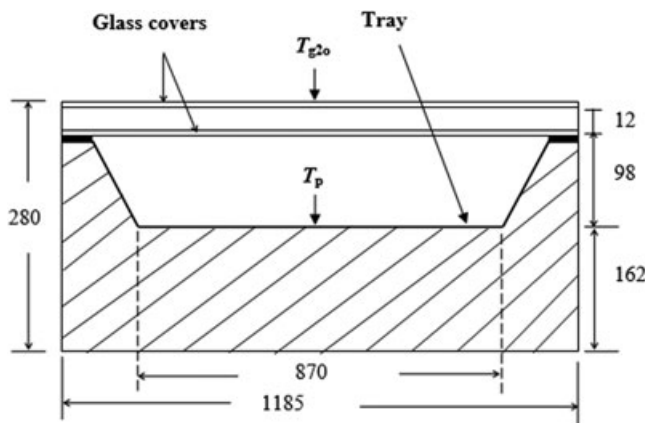

FIGURE 1 A schematic of the solar cooker considered in the present study. All dimensions are in mm. The thickness of the glass covers is 4 mm. L_1 and L_2 are equal to 260 mm ($= 98 + 262$ mm) and 12 mm, respectively

covers, and glass wool bottom. The measurement of the wind speed is carried out using a three-cup anemometer of G. Lufft make (kept beside the plate). The anemometer used is very sensitive and could respond to wind gusts of brief duration (in seconds). The anemometer cup is stationed at a vertical distance 150 mm higher than the top surface of the test plate. The measurements of solar radiation are carried out with the help of a Kipp and Zonen pyranometer (CMP-6), which had a temperature dependence of sensitivity less than 4%. Solar radiation and ambient temperature measurements are taken at the exact site of experiments. All the temperature measurements in the experiment, namely, that of the ambient, test plate, bottom insulation, and so forth; solar radiation and wind speed are recorded at an interval of 1 second through OPUS data-loggers, and later the recorded data are averaged over a duration of 10 minutes.

2.2 | Meteorological measurements

The meteorological data (ambient temperature, RH, and wind speed) are collected at the in-house weather station, located at University of Petroleum and Energy Studies, Dehradun, India. At the UPES weather station, the ambient temperature and relative humidity (RH) data are recorded for 14 months (July 2016-September 2017) using a multiplate radiation shield apparatus from Young Inc (Model 41003), which protects the temperature and RH measurements from error-producing solar radiation and precipitation. The maximum error in the measurements of temperature fall within a maximum of $\pm$0.3°C and that in the RH is within $\pm$2%. The wind speeds are measured in sync, using an ultrasonic anemometer from Young Inc (Model 81000), which gives the wind speeds within a range of 0.05 m/s (till a wind speed of 30 m/s), or accuracy of $\pm$1%.The data are collected through data-loggers and stored as data files in the weather station work station. These data files are later analyzed using MATLAB software. The hourly solar insolation data for Dehradun are obtained from 10 km gridded satellite data from the National Renewable Energy Laboratory website for Dehradun (latitude: 30.35°; longitude: 78.05°). Using the above measurements, the sky temperature is predicted using different correlations extracted from the prior literature. Finally, a MATLAB script is written to determine the solar cooker performance by solving the basic governing equations for all modes of heat transfer.

3 | ANALYSIS OF SKY TEMPERATURE

3.1 | Sky temperature and its estimation

The atmosphere can be considered to be a gray body and the atmospheric longwave irradiance in the range of 3 to 100 μm (R_{sky}) can be approximated as a fraction of the blackbody emissive power evaluated at the surface level ambient temperature (T_a). This fraction is called the effective sky emissivity, ε^2 and is expressed as

$$\varepsilon = \frac{R_{sky}}{\sigma T_a^4}, \tag{1}$$

where, $\sigma = 5.67 \times 10^{-8}$ W/m^2 K^4 is the Stefan-Boltzmann constant and R_{sky} can be estimated by approximating the sky as a blackbody and defining a sky temperature (T_{sky}) as

$$R_{sky} = \sigma T_{sky}^4. \tag{2}$$

Comparing the above two equations, the relationship between the sky temperature and the surface level ambient temperature can be written as

$$T_{sky} = \varepsilon^{1/4} T_a. \tag{3}$$

As ε ranges from 0 to 1, the effective sky temperature is lower than the surface level air temperature.[18] Usually, there are three different approaches to estimate the sky temperature: empirical methods, radiation charts, and computer program models.[5] Radiation charts are derived from experimental and theoretical radiation calculations and present the minimum, mean, and maximum monthly sky temperature in chart formats.[19] Computer program models require detailed inputs of atmospheric constituents and are considered very cumbersome, akin to using radiation charts. In contrast, empirical methods are direct and rely on measurements and atmospheric data. Hence, the current study focuses on the use of empirical methods for the determination of sky temperature and is discussed in Section 4.1.

3.2 | Governing parameters for effective sky emissivity

As evident from Equation (3) in the previous section, the sky temperature at a given ambient temperature can be computed, provided an accurate estimation of effective sky emissivity can be obtained. The sky emissivity can be estimated by taking stock of the underlying parameters behind atmospheric radiation. Atmospheric radiation emanates from the gases in the air, some of which absorb and emit in the far infrared range. Of these gases, oxygen and nitrogen constitute an enormous majority (about 99% by volume), although these two gases being transparent to such radiation, do not absorb or emit in the far infrared. Atmospheric radiation can be attributed to water vapor, carbon dioxide, ozone, and other asymmetrical molecules that exist in the atmosphere. Owing to their stability in their content and distribution along the altitude, gases like carbon dioxide, ozone, and so forth do not have much influence on the variation of atmospheric radiation received at the ground.[20] Thus, the variation in the water vapor in the atmosphere near the ground is a major contributor to the atmospheric radiation. Bliss[3] estimated that about 90% of the atmospheric radiation received at the ground level originates at an altitude less than 1 km, out of which 40% can be directly attributed to the atmosphere 10 m above the ground. As the atmospheric layer at the surface level differs from one place to another and depends upon several factors such as altitude, humidity, and so forth, it is expected that the different places would yield different correlations for calculation of atmospheric radiation. Although the effective sky temperature is always lower than the ambient air temperature due to a decrease in elevation, but the presence of clouds in the sky usually tend to increase the effective sky temperature, causing it to approach the clear-sky temperature. In general, the effective sky emissivity of the atmosphere can be expressed as a function of ambient temperature (T_a), relative humidity ($\varnothing$) and/or other meteorological variables such as partial pressure of water vapor (P_v) and dew-point temperature (T_{dp}). Apart from these primary parameters, the sky emissivity additionally also depends on the cloudiness of the sky, moisture content, and so forth. However, in the current study, we restrict our attention to the clear-sky emissivity only on measured and derived parameters as

$$\varepsilon = f(T_a, \varnothing, T_{dp}, P_v). \tag{4}$$

It is worth noting here that although the measured parameters are only ambient temperature and the relative humidity, the dew point and water vapor pressure can be derived from it based on many previous expressions published in the literature. Table 1 presents some of the expressions that have been proposed for the estimation of dew-point temperature and water vapor pressure in the literature. As these expressions look vastly different, a thorough examination of the sky temperature estimation demands that variations produced due to the usage of these different correlations be studied. For the estimation of dew-point temperature and the water vapor pressure, we choose the monthly data across winter and summer seasons. As shown in the table, the fundamental correlations suggested for dew point are denoted as F1,[21] F2,[22] F3,[23] and F4,[24] whereas those suggested for water vapor pressure are represented as F1, F3, and F5.[25]

Figure 2 presents the variation in the estimation of dew-point temperatures for both day and night during winter (data set of January 2017) and summer (data set of June 2017), respectively. First, as expected, there is a significant reduction in water vapor pressure values in winters (Figure 2a) when compared with summers (Figure 2b). Figure 2a and 2b also shows that the three proposed correlations[21-25] predict a fairly coincident value for the water vapor pressures. The dew-point variation as shown in Figure 3 has a similar trend with respect to the comparison between summer and winter months. However, the dew-point temperature across the days of the month, as proposed by different correlations do not concur with each other over a wide range of ambient temperature and humidity conditions. Figure 3 indicates that the simplified correlation proposed by Lawrence[24] predicts a consistently larger value when compared with other expressions.[21-23] The difference can range from a maximum of 13°C in the winter season (Figure 3a), to about a maximum of 8°C during summers (Figure 3b). Surprisingly, for the nighttime dew-point temperature, all the correlations converge fairly well, both for summer and winter conditions. This tends to indicate that the correlation proposed by Lawrence[24] can prove to be inaccurate for the estimation of dew-point temperature, particularly during summers or low humidity conditions. In conclusion, for the estimation of water vapor pressure, either of these correlations proposed in the literature can be used interchangeably for the estimation of sky temperature.

TABLE 1 Different correlations for prediction of dew-point temperature and water vapor pressure (T_{dp} and T_a are in °C, P_v is in Pascals, and $\varnothing$ is expressed as a fraction)

Dew-point temperature (°C)	Reference	Water vapor pressure, P_v (Pa)	Reference
$T_{dp} = \dfrac{3890.94 + 230.4(\ln(\varnothing) - (3890.94/(T_a + 230.4)))}{(3890.94/(T_a + 230.4))\ln(\varnothing)}$	F1[21]	$P_v = \varnothing \exp\left(23.3 - \dfrac{3890.94}{T_a + 230.4}\right)$	F1[21]
$T_{dp} = \dfrac{243.04 \ln(P_v/610.94)}{17.625 - \ln(P_v/610.94)}$	F2[22]	$P_v = 610.94\, \varnothing \exp\left(\dfrac{17.625 T_a}{T_a + 243.4}\right)$	F3[23]
$T_{dp} = \dfrac{5179.25}{20.519 - \ln(7.60(P_v/1,013))} - 273.15$	F3[23]	$P_v = 611\, \varnothing\, 10^{((7.5 T_a)/(T_a + 237.3))}$	F5[25]
$T_{dp} = T_a - 100\left(\dfrac{1 - \varnothing}{5}\right)$	F4[24]		

(F1-F5) refer to Fang,[21] Berger et al,[22] Alduchov and Eskridge,[23] Lawrence,[24] and Daniel,[25] respectively.
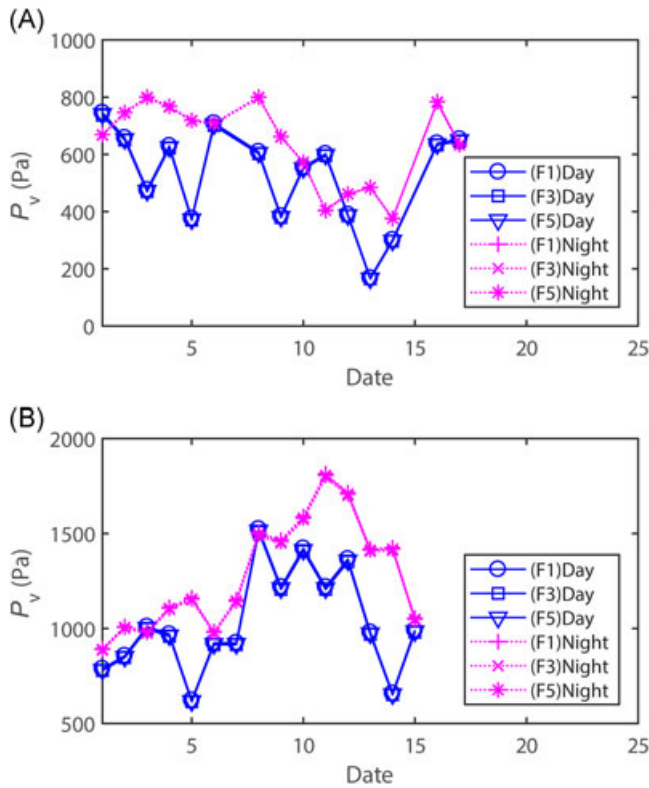
FIGURE 2 Variation in the estimation of dew-point temperature as obtained from expressions in Table 1 for 15 days during (A) winter and (B) summer months [Color figure can be viewed at wileyonlinelibrary.com]

3.3 | Models of effective sky emissivity

Within the published literature, a slew of sky temperature models and emissivity correlations that have been proposed to estimate the effective sky temperature and most of these models pertain to clear-sky conditions. To compare the effectiveness of these correlations in estimating the sky temperature and thus the performance of a solar cooker, these correlations are broadly grouped into four functional families as follows:

- Type 1: Expressions based on P_v (M1-M10[9,18,26-33]),
- Type 2: Expressions based on T_{dp} (M11-M15[1,3,22,34,35]),
- Type 3: Expressions based on T_a (and $\varnothing$) (M16-M19[36-39]),
- Type 4: Expressions based on P_v and T_a (M20-M26[40-46]).

Table 2 presents a list of all the clear-sky emissivity models in chronological order. Of all the emissivity correlations, some of these are for daytime (for instance, some specifically pertain to nighttime emission[9,31,38] while other authors have proposed separate correlations for day and night.[1,3,18,22] Apart from the correlations mentioned above, some other correlations with same functional form but different coefficients have also been reported for type 1 (eg, Raman[47]) and type 2 (Tang et al[20] and Chen et al[48]) but are not included here to avoid repetition of the similar expressions.
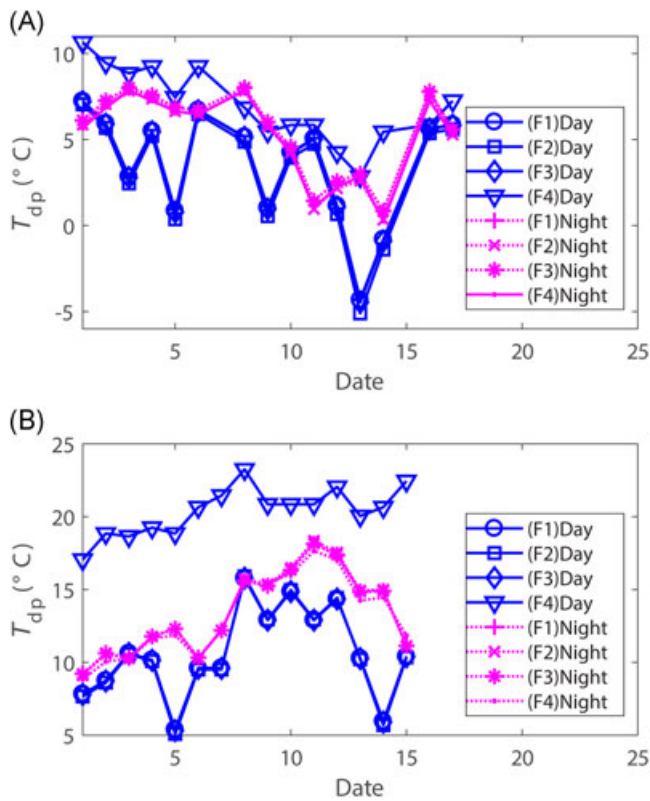
FIGURE 3 Variation in the estimation of water vapor pressures as obtained from expressions in Table 1 for 15 days during (A) winter and (B) summer months [Color figure can be viewed at wileyonlinelibrary.com]

It is necessary that the estimation and variation of sky temperatures be studied in the range of ambient temperatures and relative humidity that resembles weather conditions at the location where data are collected (Dehradun, India). The maximum and minimum temperatures observed at Dehradun are 42°C and 0°C, respectively. The relative humidity, $\varnothing$, varies between 0.1 and 1 (*RH*: 10%-100%). Thus, a mean ambient temperature of 21°C and mean $\varnothing$ of 0.55 is chosen. Thereafter, the effect of variation in $\varnothing$ at a fixed ambient temperature and effect of fluctuation in ambient temperature at a constant $\varnothing$ is studied to investigate the deviations in the prediction of clear-sky emissivity caused by the use of these different proposed emissivity models.

3.4 | Variations in sky temperature prediction by using different emissivity models

Figure 4 illustrates the effect of these variations for type 1 and type 2 models for Dehradun conditions. For both the plots of type 1, it can be clearly observed that the model M6 by Elsasser[29] significantly underestimates the emissivity values at low $\varnothing$ or T_a, whereas the M1 model by Angstrom[9] is a slight underestimate in the high $\varnothing$ or T_a range. The emissivity values predicted by type 2 models fall within a narrow band. However, significant differences between the predicted emissivity are observed for type 3 and type 4 models as shown in Figure 5. The

TABLE 2 Clear-sky atmospheric emissivity models (T_{dp} and T_a are in K, P_v is in millibar or hectopascals and $\varnothing$ is expressed as a fraction)

	References	Sky-emissivity model	Parameters	Type
M1	Angstorm[9]	$\varepsilon = C_1 - C_2 \exp(-C_3 P_v)$	$C_{1n} = 0.806$ $C_{2n} = 0.236; C_{3n} = 0.092$	1
M2	Li and Coimbra[18]	$\varepsilon = C_1 + C_2 \sqrt{P_v}$	$C_{1d}/C_{1n} = 0.598/0.633$ $C_{2d}/C_{2n} = 0.057/0.057$	1
M3	Vishwanandham and Ramanandham[26]	$\varepsilon = C_1 - C_2 \times 10^{C_3 P_v}$	$C_{1n} = 0.880$ $C_{2n} = 0.320$ $C_{3n} = -0.069$	1
M4	Centeno[27]	$\varepsilon = C_1 + C_2 \sqrt{P_v}$	$C_{1n} = 0.56$ $C_{2n} = 0.08$	1
M5	Brunt[28]	$\varepsilon = C_1 + C_2 \sqrt{P_v}$	$C_1 = 0.520$ $C_2 = 0.065$	1
M6	Elsasser[29]	$\varepsilon = C_1 + C_2 \ln P_v$	$C_1 = 0.210$ $C_2 = 0.22$	1
M7	Anderson[30]	$\varepsilon = C_1 + C_2 \sqrt{P_v}$	$C_1 = 0.680$ $C_2 = 0.036$	1
M8	Kondratyev[31]	$\varepsilon = C_1 + C_2 \sqrt{P_v}$	$C_1 = 0.660$ $C_2 = 0.040$	1
M9	Staley and Jurica[32]	$\varepsilon = C_1 (P_v)^{C_2}$	$C_1 = 0.670$ $C_2 = 0.080$	1
M10	Niemela et al[33]	$\varepsilon = C_1 + C_2 (P_v - C_3)$	$C_1 = 0.72$ $C_2 = 0.009; C_3 = 2$	1
M11	Berdahl and Fromberg[1]	$\varepsilon = C_1 + C_2 (T_{dp} - 273)$	$C_{1d}/C_{1n} = 0.727/0.741$ $C_{2d}/C_{2n} = 0.0061/0.0062$	2
M12	Bliss[3]	$\varepsilon = C_1 + C_2 (T_{dp} - 273)$	$C_{1d}/C_{1n} = 0.8004/0.8$ $C_{2d}/C_{2n} = 0.00396/0.004$	2
M13	Berger[22]	$\varepsilon = C_1 + C_2 (T_{dp} - 273)$	$C_{1d}/C_{1n} = 0.752/0.770$ $C_{2d}/C_{2n} = 0.0048/0.0038$	2
M14	Clark and Allen[34]	$\varepsilon = C_1 + C_2 (T_{dp} - 273)$	$C_1 = 0.787$ $C_2 = 0.0028$	2

(Continues)

TABLE 2 (Continued)

	References	Sky-emissivity model	Parameters	Type
M15	Berdahl and Martin[35]	$\varepsilon = c_1 + c_2(T_{dp} - 273)/100 + c_3[(T_{dp} - 273)/100]^2$	$C_1 = 0.711$ $C_2 = 0.560$; $C_3 = 0.73$	2
M16	Swinbank[36]	$\varepsilon = C_1 T_a^{C_2}$	$C_1 = 9.284 \times 10^{-6}$ $C_2 = 2$	3
M17	Sloan et al[37]	$\varepsilon = C_1 + (C_2 \varnothing / T_a)\exp[C_3(T_a - 273.15)/T_a - C_4]$	$C_1 = 0.371$; $C_2 = 0.255$ $C_3 = 17.67$; $C_4 = 29.65$	3
M18	Idso and Jackson[38]	$\varepsilon = 1 - C_1\exp[C_2(273 - T_a)^2]$	$C_1 = 0.261$ $C_2 = -0.000777$; $C_3 = 2$	3
M19	Carmona et al[39]	$\varepsilon = C_1 + C_2 T_a + C_3 \varnothing$	$C_1 = -0.34$ $C_2 = 0.00336$; $C_3 = 0.14$	3
M20	Brutsaert[40]	$\varepsilon = C_1(P_v/T_a)^{C_2}$	$C_1 = 1.240$ $C_2 = 1/7$	4
M21	Satterlund[41]	$\varepsilon = C_1[1 - \exp(-P_v^{T_a/C_2})]$	$C_1 = 1.080$ $C_2 = 2016$	4
M22	Idso[42]	$\varepsilon = C_1 + C_2 P_v \exp(C_3/T_a)$	$C_1 = 0.700$ $C_2 = 5.950 \times 10^{-5}$ $C_3 = 1500$	4
M23	Prata[43]	$\varepsilon = 1 - (1 + C_1 P_v/T_a)\exp(-\sqrt{(C_2 + C_3 P_v/T_a)})$	$C_1 = 46.5$ $C_2 = 1.2$; $C_3 = 139.5$	4
M24	Dilley and O'Brien[44]	$\varepsilon = \left[C_1 + C_2\left(\frac{T_a}{273.16}\right)^2 + C_3\sqrt{w/25}\right]/\sigma T_a^4$; $w = 4.65 \frac{P_v}{T_a}$	$C_1 = 59.38$ $C_2 = 113.7$ $C_3 = 96.96$	4
M25	Crawford and Douchon[45]	$\varepsilon = [C_1 + C_2 \sin\{(m + 2)\pi/6\}]\left(\frac{P_v}{T_a}\right)^{1/7}$	$C_1 = 1.22$ $C_2 = 0.06$ $m = 1\text{-}12(1:\text{ January}; 12:\text{ December})$	4
M26	Iziomon et al[46]	$\varepsilon = 1 - \left[C_1 \exp\left(\frac{C_2 P_v}{T_a}\right)\right]$	$C_1 = 0.35$ $C_2 = -10$	4

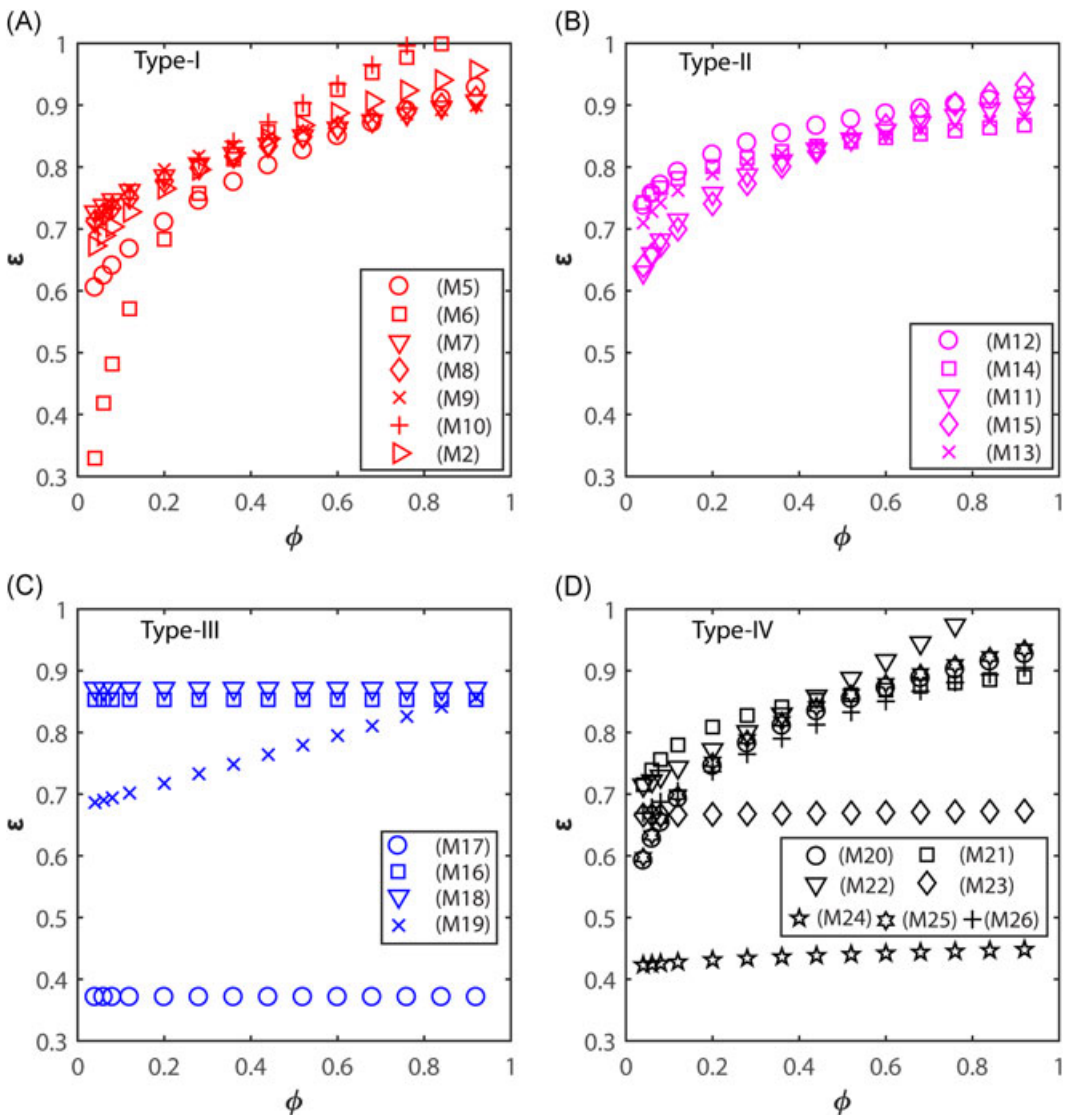Correlations M1, M2, M3, M4, M11, and M12 pertain to nighttime correlations.

FIGURE 4 Variation of clear daytime sky emissivity, ε with relative humidity expressed as a fraction for a fixed mean ambient temperature of 30°C using emissivity correlations of (A) type 1, (B) type 2, (C) type 3, and (D) type 4 [Color figure can be viewed at wileyonlinelibrary.com]

curves for type 3 indicate that there is a perfect resemblance between the models of Swinbank[36] and Idso and Jackson.[38] Although a number of previous studies have suggested the use of Swinbank correlation for the estimation of clear-sky emissivity, a significant difference is observed between Swinbank correlation and other type 3 models, particularly with Sloan et al.[37] Similarly, the models of Prata[43] and Dilley and O'Brien[44] predict considerably different results when compared with other models of type 4. Thus, in total, five models can be identified that yield drastically different emissivity values: M1, M6, M16, M23, and M24 and the errors associated in the sky temperature estimation using these correlations, which need to be investigated.
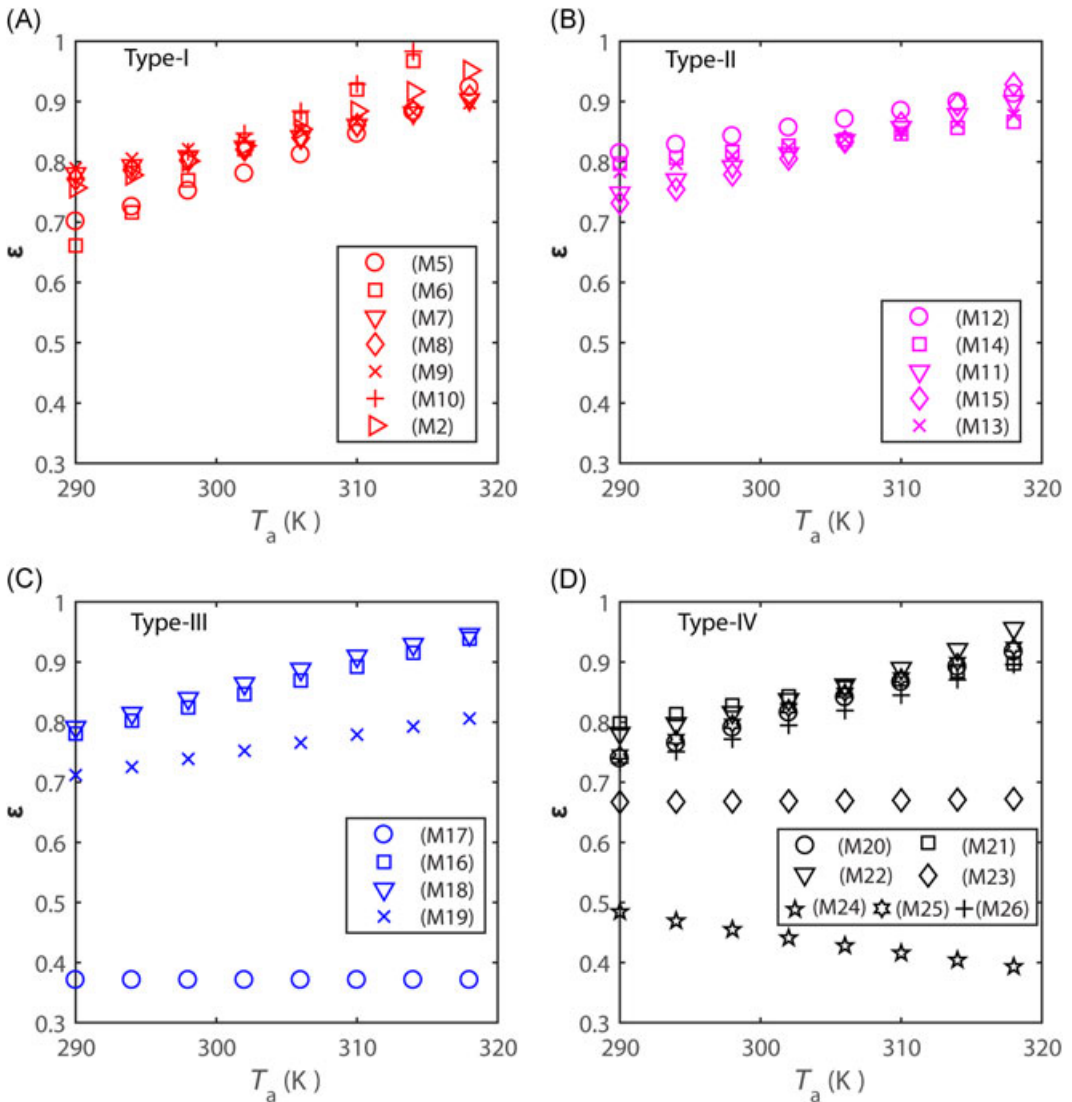
FIGURE 5 Variation of clear daytime sky emissivity, ε with ambient temperature at a mean relative humidity of 0.40 using emissivity correlations of (A) type 1, (B) type 2, (C) type 3, and (D) type 4 [Color figure can be viewed at wileyonlinelibrary.com]

Next, as far as nighttime sky emissivity is concerned, there are six correlations proposed by earlier authors, which are enlisted in Table 2 (M1, M2, M3, M4, M11, and M12). For the nighttime sky emissivity, as shown in Figure 6, as $\varnothing$ increases, the band of emissivity values increases between different correlations, whereas at a fixed $\varnothing$, different range of temperatures does not seem to significantly alter the deviation in the estimation of nighttime sky emissivity. Next, we consider the variation in the estimation of sky temperature by these different correlations for both day and night conditions during different seasons.
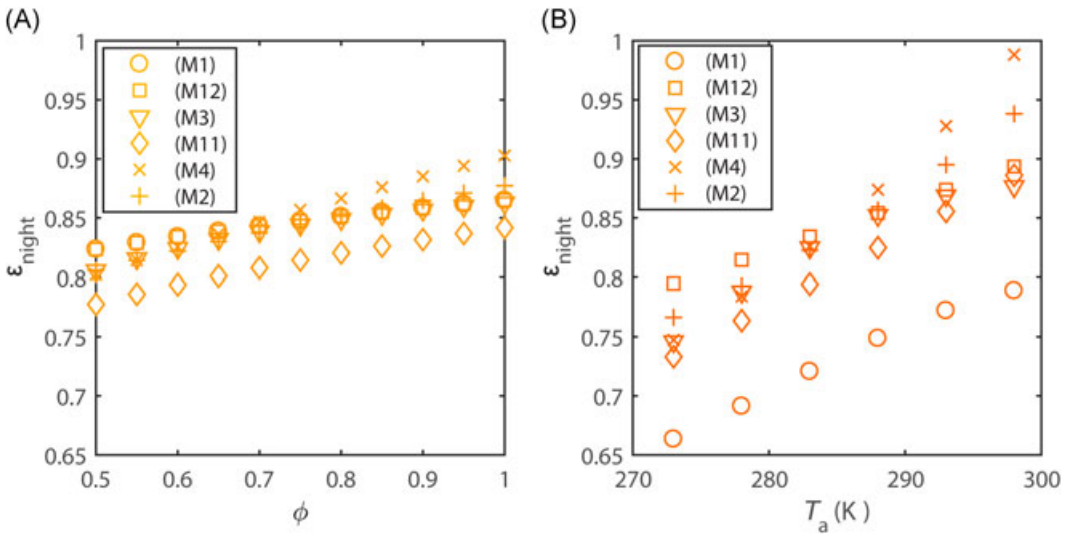
FIGURE 6 Variation of nighttime sky emissivity, ε with (A) relative humidity expressed as a fraction for a fixed mean ambient temperature of 16°C and (B) ambient temperature at a mean relative humidity of 0.90 [Color figure can be viewed at wileyonlinelibrary.com]

3.5 | Day-night and seasonal variations in sky temperature

Figure 7 illustrates the variation of the sky temperatures as predicted by these correlations for winter, summer, and monsoon conditions in Dehradun. For the purpose of analysis in our study, 1 PM and 1 AM were chosen to correspond to the daytime and nighttime conditions, respectively. This selection of a fixed daytime was backed by the prior reports in the literature[49] on solar cookers, which had shown that the cooker plate temperature generally keeps on increasing with a rise in insolation beginning from the morning, reaching a quasi-static state a little before 1 PM during the day. Thus, the daytime variation in sky temperature prediction is shown as a reference in Figure 7. A number of things can be pointed out based on our observations from these figures. First, for all the seasons, it can be clearly seen that the deviation in the sky temperature is considerable for any given day considering the formulations listed in Table 2. This clearly indicates the enormous errors one might encounter while calculating the sky temperatures in different seasons. Irrespective of the fact whether this has a significant bearing on the first-figure-of-merit for solar cooker, this is an important finding, particularly for other applications such as aerostats or the radiative cooling of buildings and so forth. As evident from these figures, the daytime T_{sky} values may span a range of 70°C or more. However, the nighttime sky temperature lies within a fairly narrow band and is greater than the daytime sky temperature, meaning that the night sky is more emissive than the day sky. Apart from the minor fluctuations, the mean sky temperature is close to 0°C during winters and about 15 to 20°C during summers or monsoons. The average of these mean sky temperatures yield a value of -0.25°C for winters, 16.12°C for summers, and 17.48°C for monsoons. The variance in the sky temperature predicted by different formulations is displayed in Figure 8. It shows that the variance in sky temperatures is greatest for monsoon months and least for winter months. There are some other points worth noting in Figure 7. The difference between ambient temperature and sky temperature is largest in the winter months. This difference reduces slightly in the summer (the ambient temperature moves closer to the T_{sky} band) and merges
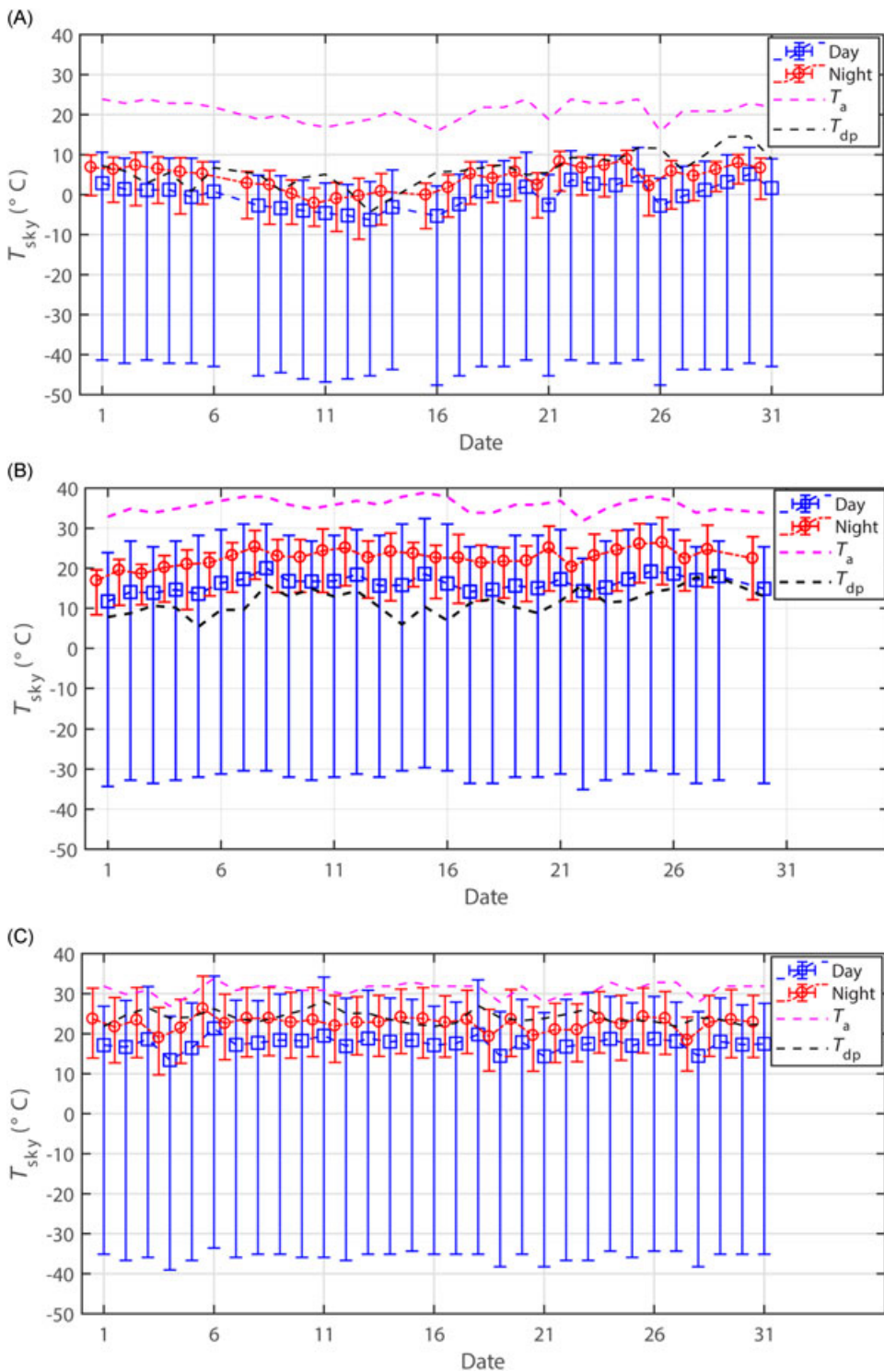
FIGURE 7 Range of variation in the day and nighttime sky temperatures as predicted from correlations M1-M26 in Table 2 for the data set of (A) winter (January 2017), (B) summer (May 2017), and (C) monsoon (August 2017). The light magenta and dark black dashed lines indicate the daytime ambient temperature and dew-point temperature for the same data set. The error bars for the nighttime sky temperatures are displaced slightly to the left for clarity [Color figure can be viewed at wileyonlinelibrary.com]
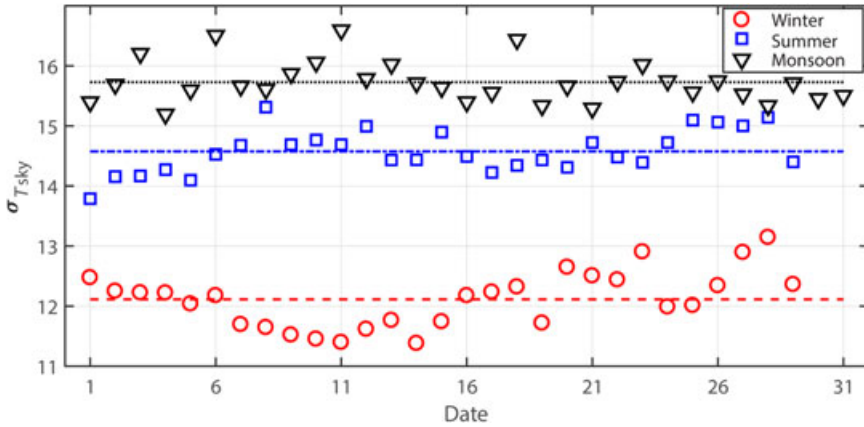
FIGURE 8 Standard deviation in the sky temperature for different seasons [Color figure can be viewed at wileyonlinelibrary.com]

with the T_{sky} band for the monsoons. Further, except for the summer months, when the dew point is quite low when compared with the ambient temperature (or sky temperature), the sky temperature is close to the dew-point temperature.

4 | EFFECT OF SKY TEMPERATURE VARIATION ON SOLAR COOKER PERFORMANCE

To evaluate the thermal performance of box-type solar cooker as per the Indian standard, two figures of merit have been suggested by Mullick *et al.*[17] The first-figure-of-merit, F_1 is obtained by performing the outdoor experiments in the clear sunshine days, around solar noon on the empty solar box cooker to be tested. F_1 is a function of optical efficiency (η_o) corresponding to the glazing and absorber system used and also the overall coefficient of heat loss U_L, of the solar cooker:

$$F_1 = \eta_o/U_L. \tag{5}$$

4.1 | Calculation of optical efficiency (η_o)

As far as the optical efficiency of a box-type solar cooker is concerned, it is different for the beam component and diffuse component of solar radiation. Thus, the effective optical efficiency can be calculated as

$$\eta_o = \eta_{ob}R_b + \eta_{od}R_d, \tag{6}$$

where η_{ob} and η_{od} are optical efficiency for the beam component and diffuse component of solar radiation, respectively. R_b and R_d denote the ratio of beam radiation to the total radiation and ratio of diffuse radiation to the total radiation, respectively. A simple procedure suggested by Duffie and Beckman[50] has been followed to calculate the optical efficiency. The optical efficiency for the beam component of the solar radiation is determined by calculating the angle of incidence of the beam radiation for the specific time and day for a particular location. In contrast, the optical efficiency for the diffuse

component is calculated and used corresponding to an effective angle of incidence of 60°, similar again to Duffie and Beckman.[50]

4.2 | Calculation of heat transfer factor (U_L)

The overall heat loss coefficient (U_L) of a box-type solar cooker depends upon the cooker design parameters. The overall heat transfer factor, U_L, is the sum of top heat transfer factor (U_t), bottom heat transfer factor U_b, and side heat transfer factor U_s:

$$U_L = U_t + U_b + U_s. \tag{7}$$

Figure 9 shows a schematic of the various heat transfer modes at play in the operation of a solar cooker. Both the glass covers have a conduction resistance owing to which the temperatures at both the surfaces of both the glass plates are not identical. Further, there is a convection and radiation exchange between the absorber plate and the first glass cover, as well as between the first and second glass covers. The second glass cover exchanges heat with the surroundings through convection as well as radiates heat to the atmosphere through radiation. Heat transfer occurs in all directions—top, bottom, and sides. For evaluating the top heat loss factor, individual heat transfer coefficients for convection and radiation should be calculated. The bottom and side heat loss coefficients have been combined together and reported equal to 0.85 W/m^2 K for the solar cooker under consideration, in the prior studies of Khan.[51] Hence, once the top heat loss factor is determined, the overall heat transfer coefficient can be calculated.

Figure 10 presents a simplified thermal resistance network for the box-type solar cooker. Under steady-state conditions, the rate of heat loss per unit area from the absorber plate to the inner glass cover:

$$Q_t'' = \frac{(T_p - T_{1o})}{[L_g/k_g + (h_{cpg1} + h_{rpg1})^{-1}]}$$
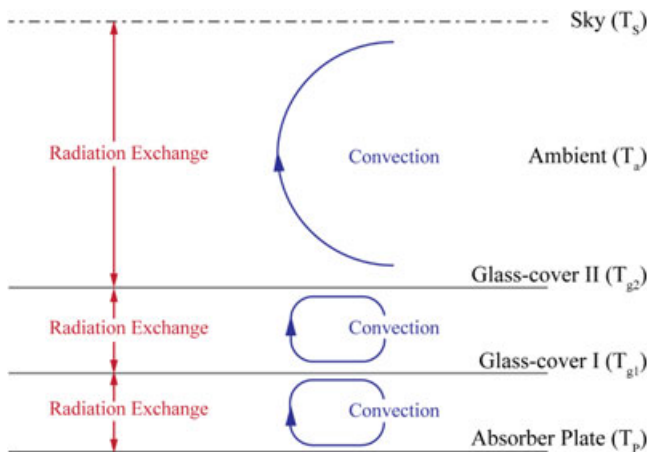
or

FIGURE 9 Heat transfer mechanism through the cover system with two glass covers [Color figure can be viewed at wileyonlinelibrary.com]
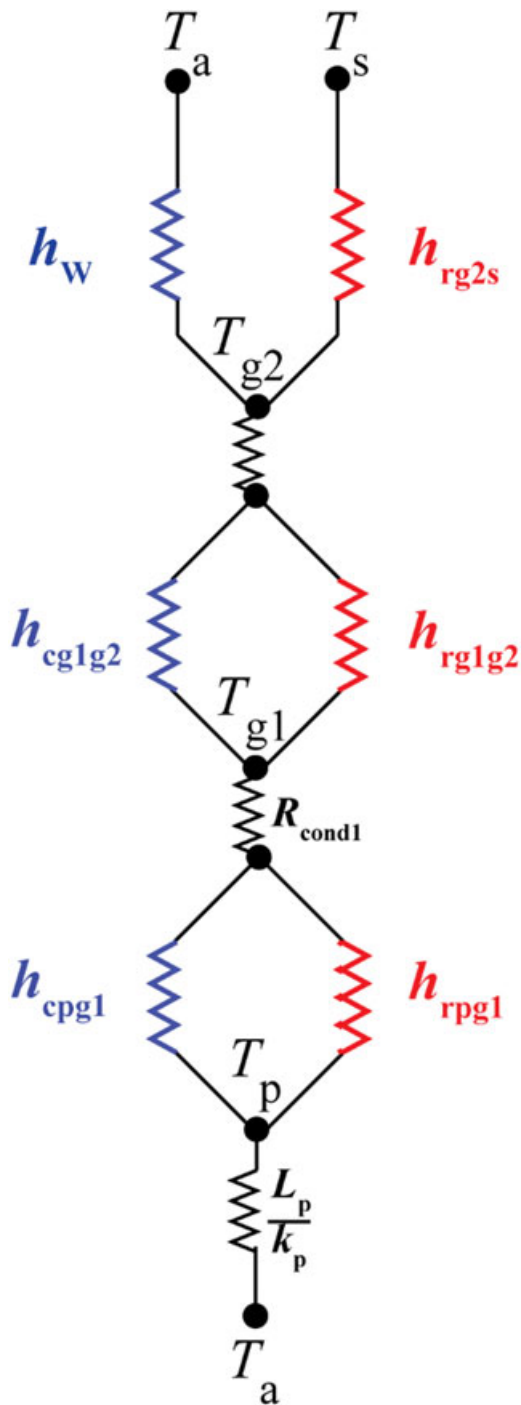
FIGURE 10 Thermal network for double-glazed solar cooker in terms of conduction convection and radiation. Note that the conduction resistances of the glass covers are assumed as negligible [Color figure can be viewed at wileyonlinelibrary.com]

$$(T_p - T_{1o}) = Q_t'' [L_g/k_g + (h_{cpg1} + h_{rpg1})^{-1}], \tag{8}$$

where L_g and k_g denote the thickness and thermal conductivity of the glass cover, respectively, and equal to 4 mm and 1.36, respectively (heat transfer coefficients are described after Equation (11)). Similarly, between the inner glass cover to the outer glass cover,

$$(T_{1o} - T_{2o}) = Q_t'' [L_g/k_g + (h_{cg1g2} + h_{rg1g2})^{-1}]. \tag{9}$$

This heat transfer should also equal the heat exchange between the outer glass cover to the atmosphere at the steady state:

$$Q_t'' = (h_{rg2s} + h_w)(T_{2o} - T_a),$$

$$(T_{2o} - T_a) = Q_t''(h_{rg2s} + h_w)^{-1}. \tag{10}$$

Adding Equations (9,10,12), we get

$$(T_p - T_a) = Q_t'' [2L_g/k_g + (h_{cpg1} + h_{rpg1})^{-1} + (h_{cg1g2} + h_{rg1g2})^{-1} + (h_{rg2s} + h_w)^{-1}], \tag{11}$$

where h_{rpg1} and h_{cpg1} are the radiative and convective heat transfer coefficient from absorber plate to inner glass cover and is calculated as

$$h_{rpg1} = \left(\frac{\sigma}{(1/\varepsilon_p) + ((1/\varepsilon_g) - 1)} \right) (T_p^2 + T_{g1}^2)(T_p + T_{g1}), \tag{12}$$

$$h_{cpg1} = \frac{K_1 \times Nu_1}{L_1}. \tag{13}$$

In Equations (12) and (13), the value of the emissivity of plate (ε_p) and glass (ε_g) are 0.95 and 0.88, respectively. L_1 equals 260 mm and thermal conductivity K_1 is computed at a mean temperature of $(T_p + T_{g1})/2$.

Next, the radiative and convective heat transfer coefficient from the inner glass cover to the outer glass cover, h_{rg1g2} and h_{cg1g2}, are calculated as

$$h_{rg1g2} = \left(\frac{\sigma}{(2/\varepsilon_g) - 1} \right) (T_{g1}^2 + T_{g2}^2)(T_{g1} + T_{g2}), \tag{14}$$

$$h_{cg1g2} = \frac{K_2 \times Nu_2}{L_2}. \tag{15}$$

In Equations (14) and (15), the value of the emissivity of glass (ε_g) and L_2 equal 0.88 and 12 mm, respectively, and the thermal conductivity K_1 is computed at a mean temperature of $(T_{g2} + T_{g1})/2$.

Finally, the radiative heat transfer coefficient from the outer glass cover to the atmosphere h_{rg2s} is computed as

$$h_{rg2s} = (\sigma \varepsilon_g) \frac{(T_{g2}^4 - T_{sky}^4)}{T_{g2} - T_{sky}}. \tag{16}$$

Further, both Nu_1 and Nu_2 can be evaluated according to the standard expressions for natural convection in an enclosure, given as

$$Nu = \begin{cases} 1 & Ra < 1708, \\ 1 + \left[\left(1.44 \left(1 - \frac{1708}{Ra} \right) \right) \right] \left[1 - \frac{1708}{Ra} (\sin 1.8\beta)^{1.6} \right], & 1708 < Ra < 5830, \\ 1 + \left[\left(1.44 \left(1 - \frac{1708}{Ra} \right) \right) \right] \left[1 - \frac{1708}{Ra} (\sin 1.8\beta)^{1.6} \right] + \left[\left(\frac{Ra}{5830} \right)^{1/3} - 1 \right], & Ra > 5830, \end{cases} \tag{17}$$

where Ra represents the Rayleigh number and β denotes the inclination of the cooker with respect to horizontal,[52] which equals zero in our experiments. For a quiescent ambient, the value of h_w has been measured by Kumar and Mullick as 10.[53] Moreover, the temperature difference between absorber plate and the ambient can also be written in terms of the heat transfer rate in the upward direction and the top heat transfer coefficient U_t as

$$(T_p - T_a) = Q_t'' / U_t. \tag{18}$$

By comparing Equations (11) and (18), we get a final expression for top heat loss coefficient as

$$U_t = [2L_g/k_g + (h_{cpg1} + h_{rpg1})^{-1} + (h_{cg1g2} + h_{rg1g2})^{-1} + (h_{rg2s} + h_w)^{-1}]^{-1}. \tag{19}$$

It is worth mentioning here that although the dependence of U_t upon T_{sky} is not quite apparent from the above equation, actually the T_{sky} does appear in the h_{rg2s} term. Thus, it is expected that variability in the estimation of U_t will yield varying values of U_t, and thereby F_1. However, to determine U_t, prior knowledge of T_p, T_a, and h_w is essential. T_a can be found out from the meteorological data from the weather station or from experimental measurements made near the solar cooker. The wind heat transfer coefficient is dependent upon the wind speed and can be calculated from the correlations given in the prior literature,[53] once the wind speeds are measured. However, to estimate the fluctuation in F_1 across different seasons and different climatic regions, it is necessary that U_t be known for these different cases. Further, the determination of U_t requires that the plate temperature be expressed in terms of other measurable parameters, such as T_a and H_s. Accordingly, a set of experiments on solar cookers were performed on different dates spread over a period of 3 months and all the relevant parameters were measured. The experimental measurements and the subsequent analysis are presented in the next section.

4.3 | Experiments on solar cookers for determination of absorber plate temperature

For the determination of absorber plate temperature, a systematic set of experiments are conducted and plate temperatures are measured for a wide range of conditions for three different months, as shown in the Table 3 (T_p and T_a are in K). Although there is no control over the plate temperature in a solar cooker and its operation is transient, a quasi-steady state is attained when the stagnation temperature is achieved. The recorded data correspond to the instant when such a stagnation temperature is achieved.

To relate the absorber plate temperature to other relevant parameters of a solar cooker for the fixed location (where the experiments are conducted), a simple analysis using Buckingham Pi theorem yields two dimensionless groups: nondimensional plate temperature $\theta'_p = T_p/(H_s/h_w)$, and nondimensional ambient temperature, $\theta'_a = T_a/(H_s/h_w)$ which are related as

$$\theta'_p = f(\theta'_a). \tag{20}$$

For a quiescent ambient, the value of h_w has been measured by Kumar and Mullick as 10, and the nondimensionless groups can be expressed as $\theta'_p = h_w\theta_p$ and $\theta'_a = h_w\theta_a$, where $\theta_p = T_p/H_s$ and $\theta_a = T_a/H_s$, respectively. Further, treating h_w as a constant for quiescent ambient, a linear regression is applied on the experimentally measured data to determine an equation between θ_p and θ_a. The regression analysis shows a linear equation of the form shown as follows:

TABLE 3 Experimentally recorded data for solar cookers and comparison of measured and predicted nondimensional plate temperatures

Date	T_a	H_s	T_p	T_{1i}	T_{1o}	T_{2i}	T_{2o}	$\theta_{p,meas}$	$\theta_{p,pred}$
February 27	27.29	785.33	122.03	92.88	90.19	58.68	56.16	0.504	0.504
March 5	27.89	867.69	132.14	104.86	99.98	64.30	63.51	0.467	0.467
March 6	24.51	950.08	135.28	105.86	99.20	60.18	58.98	0.430	0.432
March 7	26.07	920.59	134.69	107.11	99.14	64.28	61.05	0.443	0.444
March 8	28.08	905.30	136.97	108.90	101.32	68.19	65.05	0.453	0.452
March 17	27.15	876.29	137.03	108.08	102.23	66.51	64.24	0.468	0.463
March 23	28.43	960.67	143.35	113.65	106.41	69.39	66.18	0.434	0.432
April 2	33.32	969.61	147.34	117.61	110.98	74.58	71.45	0.434	0.434
April 10	36.44	973.36	150.14	121.63	113.06	77.62	74.50	0.435	0.437
April 11	38.86	970.54	151.63	124.08	115.44	79.96	77.38	0.438	0.441
April 12	38.04	944.49	148.57	120.99	113.37	78.31	75.70	0.447	0.449
April 26	39.08	878.32	146.42	119.08	111.46	78.46	76.44	0.478	0.476
May 3	37.93	834.21	135.95	105.76	102.22	69.03	65.07	0.491	0.494
May 5	39.10	910.09	145.25	116.51	109.42	75.20	71.75	0.460	0.463
May 10	39.64	851.00	141.16	116.12	108.64	76.88	71.90	0.487	0.489

All temperatures are recorded in °C and H_s insolation is recorded in W/m². Temperatures T_{1i}, T_{1o}, T_{2i}, and T_{2o} are shown in Figure 2.

$$\theta_{\mathrm{p}} = \varphi\theta_{\mathrm{a}} + \omega, \tag{21}$$

where the values of φ and ω are determined to be 1.045 and 0.1037, respectively. The goodness of fit is indicated by an R^2 value of 0.991, suggesting that a linear correlation indeed exists between θ_{p} and θ_{a}. The difference between the experimentally measured plate temperature and that predicted by the regression equation can be quantified in terms of root-mean-square error (RMSE) and mean-absolute-percentage error (MAPE), which are defined as follows:

$$RMSE = \left[\frac{\sum_{i=1}^{N} (\theta_{pi,\,\mathrm{pred}} - \theta_{pi,\,\mathrm{meas}})}{N} \right]^{0.5}, \tag{22}$$

$$MAPE = \frac{1}{N} \sum_{i=1}^{N} \frac{|\theta_{pi,\,\mathrm{pred}} - \theta_{pi,\,\mathrm{meas}}|}{\theta_{pi,\,\mathrm{meas}}}, \tag{23}$$

where $\theta_{pi,\mathrm{pred}}$ and $\theta_{pi,\mathrm{meas}}$ are ith predicted and measured nondimensional plate temperatures, respectively, and N is the number of data points. The calculation of RMSE and MAPE yields a low value of 0.0023 and 0.0038, respectively. Figure 11 further illustrates that the plate temperatures predicted by the proposed equation and the experimentally measured plate temperatures are in close proximity to each other. Finally, using the proposed correlation in Equation (21) with its coefficients, the absorber plate temperatures can be obtained for different weather conditions, provided total solar irradiance is known.

Figure 12 shows instantaneous measurements of total solar irradiance, H_{s} for the three seasons on the first day of the respective month. Similarly, with the instantaneous solar irradiance data known for each day, the absorber plate temperatures are derived from Equation (21) as
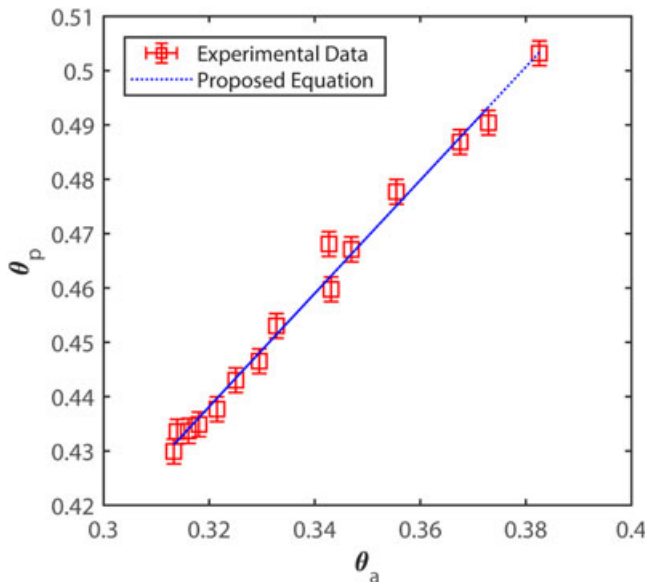

FIGURE 11 Comparison of experimental data and the prediction of θ_{p} by the proposed Equation (21). The error bars on the experimental data denote RMSE values as indicated in Equation (22) [Color figure can be viewed at wileyonlinelibrary.com]
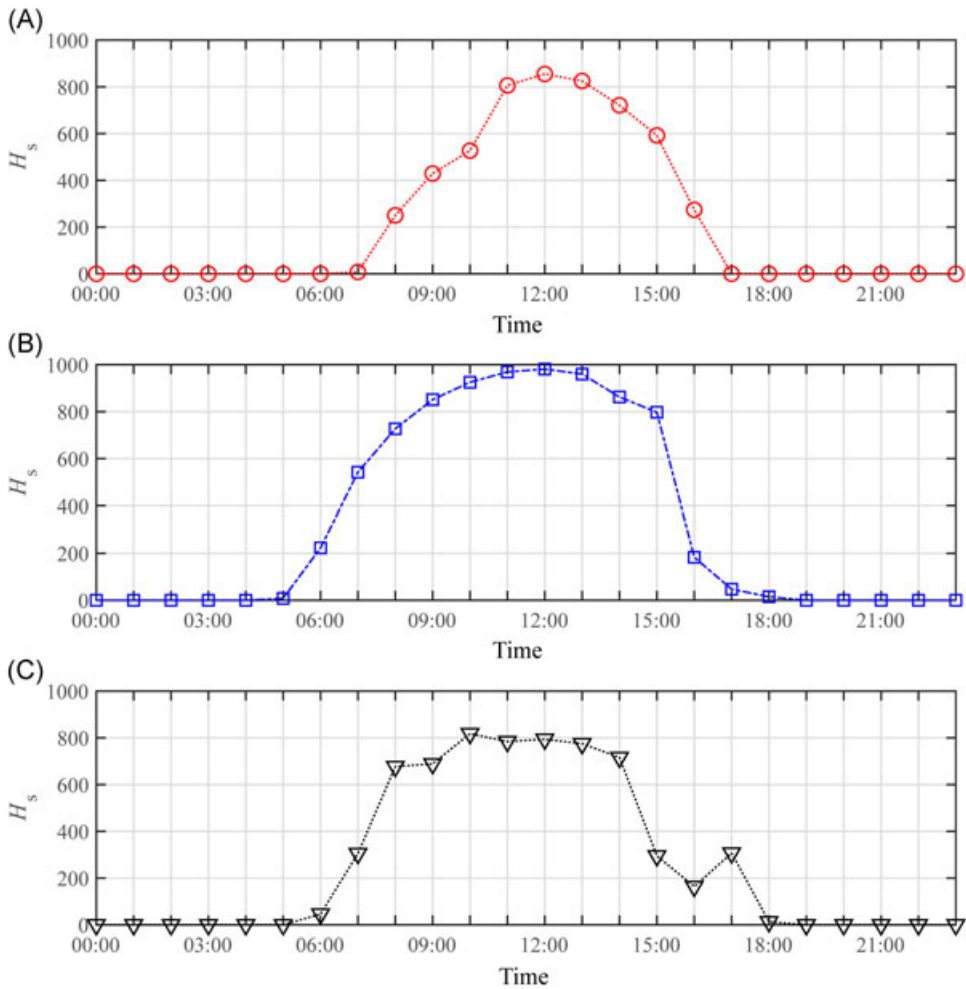
FIGURE 12 Total instantaneous solar irradiance on the first day of the month for (A) winter, (B) summer, and (C) monsoon [Color figure can be viewed at wileyonlinelibrary.com]

$T_p = 1.045 T_a + 0.1037 H_s$. Along with the meteorological variables such as ambient temperature and wind heat transfer coefficient, the top heat loss coefficient is estimated. The addition of bottom and sides heat loss factors, given as $0.85 \, \text{W/m}^2 \, \text{K}$ by Khan,[44] yields the total heat loss factor. Finally, the ratio of the optical efficiency and total heat loss coefficient yields F_1.

4.4 | Variations in F_1 for solar cookers across seasons: Effects of sky temperature

Figure 13 shows the variation in F_1 for Dehradun under winter, summer, and monsoon months, respectively, along with error bars indicating the deviation caused by the different estimations of sky temperature as per the sky-emissivity models are shown in Table 2. It can be observed that that the superimposed error bars are quite small and calculations indicate that the maximum variation in F_1 by using different correlations of the sky temperature is of the order of 3%. Even these small variations are seen to increase from winter to summer to monsoon months, as evident from Figure 13a and 13b. As far as the mean value of F_1 is concerned, it is
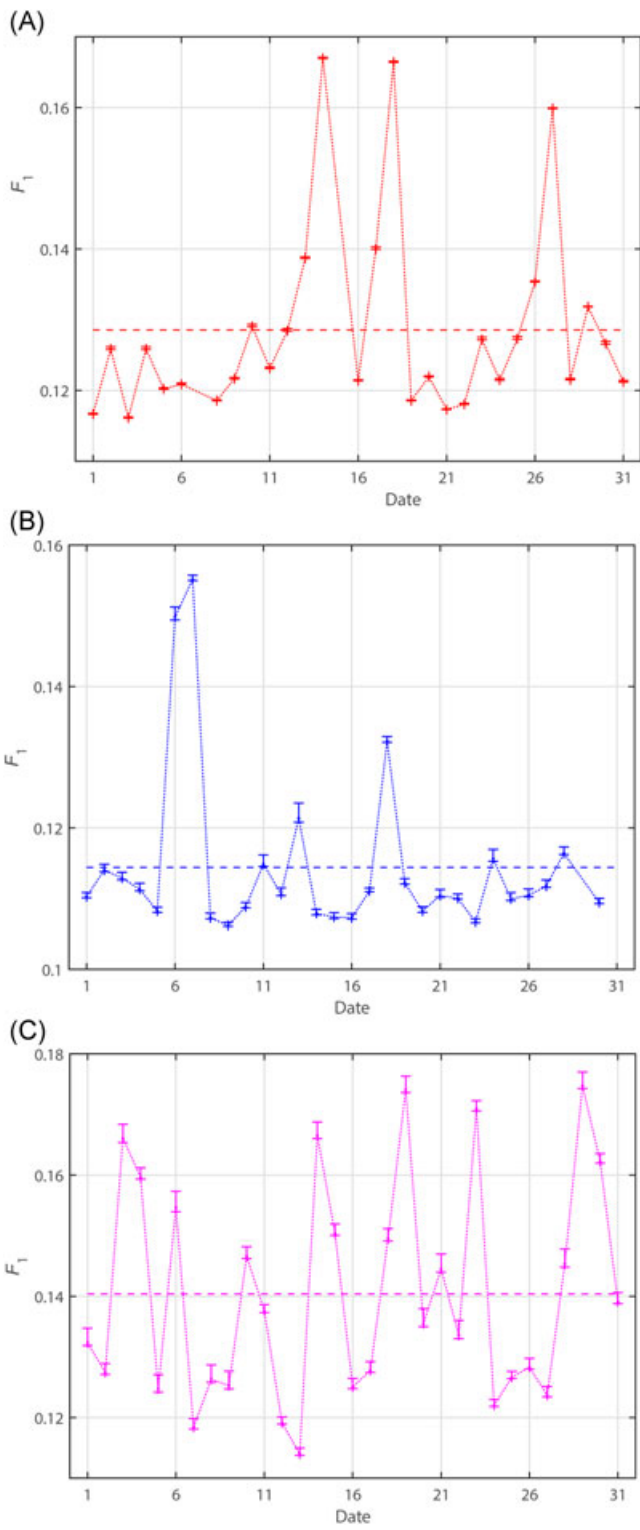
FIGURE 13 Continued.

TABLE 4 Indian cities with different daytime climatic conditions for summer conditions (May 2017)

Climate type	City	T_a (°C)	∅	H_s (W/m^2) Min-mean-max
Extreme hot-dry	Jaisalmer	39-47	0.04-0.21	560-960-982
Moderate	Bangalore	30-36	0.25-0.59	354-916-989
Cold	Srinagar	19-30	0.16-0.55	204-819-957

observed to be the lowest in the summer months, that is, around 0.115, although the values were less than 0.11 for the majority of days and stayed above 0.12 for about 4 days. During winter months, the value of F_1 increased to an average value of 0.13 and above 0.115 for all days. During winter months, F_1 value stayed above 0.14 for about 4 days in the chosen month.

The fluctuations in F_1 increased during monsoon months, when the humidity is typically high. Figure 13c shows that during monsoon months, F_1 values exceed the reported values of 0.12–0.14 for over 2 weeks. The mean F_1 values for the monsoon months is observed to be greater than 0.14. Hence, our observations indicate that F_1 does not stay constant over different days in a season. Not only it varies across the seasons beyond the suggested values of 0.12 to 0.14, even in a single month drastic variations are observed above the minimal F_1. The maximum percentage variation in F_1 about its mean value, that is, $\Delta F_1/F_1$ is about 39.8% during the winter months, 37.8% in the summer months, and around 40.7% in the monsoon months.

4.5 | Variations in F_1 for solar cookers across different climatic regions

Finally, variations in F_1 in the same season but different climatic regions in India are explored. Table 4 enlists three climate types in India with an example of an Indian city facing that climate type. Corresponding to each city, daily ambient temperature and relative humidity data are obtained from the "weather underground" whereas the insolation data have been obtained from the NREL website. Mullick et al[17] had proposed a figure-of-merit F_1, as a parameter that is independent of climatic variables, to permit evaluation of solar cookers and to facilitate comparisons between solar cookers operating at different locations. Hence, we tested out the fluctuation in F_1 values for different Indian climatic conditions in May 2017 for some of the Indian cities listed in Table 4. Figure 14 illustrates the variation in F_1 for different climatic conditions during the same time of the year. It can be clearly seen that the F_1 values lie in the range of 0.10 to 0.15 and as the climate varies from cold to moderate to extremely hot climate, F_1 successively keeps on decreasing. The mean F_1 values for Srinagar, Bangalore, and Jaisalmer lie around 0.13, 0.112, and 0.106, respectively. This shows that unlike the prior literature, where the first-figure-of-merit for a box-type solar cooker is treated as independent of climate, our study reveals a systematic dependence of F_1 upon the climatic condition as well.

◀

FIGURE 13 Variation in first-figure-of-merit of solar cooker, F_1 for the (A) winter (January 2017), (B) summer (May 2017), and (C) monsoon (August 2017). Small error bars superimposed on the marker symbols indicate the variation in F_1 caused due to the deviations in sky temperature estimation. Dashed horizontal lines indicate the mean value for the entire month [Color figure can be viewed at wileyonlinelibrary.com]
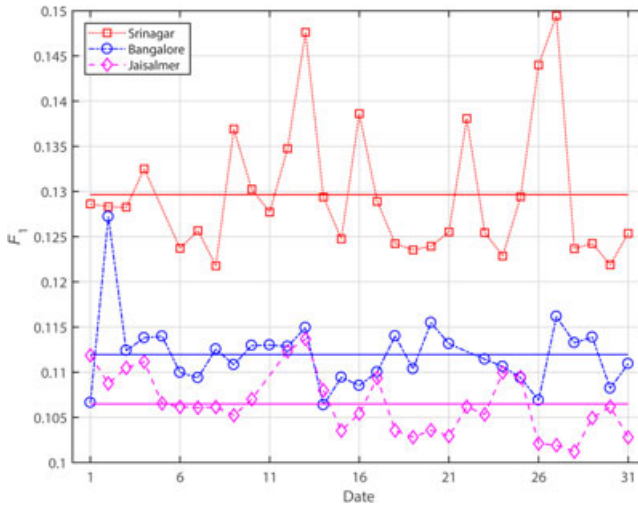
FIGURE 14 Variation of F_1 and in summer (May 2017) for different climatic regions in India [Color figure can be viewed at wileyonlinelibrary.com]

5 | CONCLUSIONS

In summary, we have studied the different factors that lead to the variability in the first-figure-of-merit of solar cookers (or the solar cooker performance) including the errors involved in the determination of sky temperature using different expressions suggested in the prior literature. In the current work, 26 different correlations proposed by prior researchers ranging from 1915 to 2017 are chosen and the sky temperature is estimated for different weather conditions. Overall, this study showed that although the errors encountered due to the sky temperature may have a nominal effect on solar cooker performance prediction, yet the influence of different seasons and weather conditions may have a prominent bearing on solar cooker performance. This deviation can be quantified in terms of F_1 exceeding beyond its usual suggested values by Mullick et al. It can be concluded that F_1 does show a dependence upon the local climate of operation. Although the erroneous sky temperature estimation can produce a maximum error of only 3% in predicting the first-figure-of-merit for solar cookers, it is possible that this result may have a more serious bearing in studies such as radiative cooling of buildings or thermal behavior of aerostats.

ORCID

Ashish Karn http://orcid.org/0000-0003-0671-4285

REFERENCES

1. Berdahl P, Fromberg R. The thermal radiance of clear skies. *Sol Energy*. 1982;29:299-314.

2. Algarni S, Darin N. Survey of sky effective temperature models applicable to building envelope radiant heat transfer. *ASHRAE Trans*. 2015;121:351.

3. Bliss RW. Atmospheric radiation near the surface of the ground: a summary for engineers. *Sol Energy*. 1961;5:103-120.

4. Clark G. Passive/hybrid comfort cooling by thermal radiation. *Passive Cooling*. Miami Beach: American Section of the International Solar Energy Society; 1981.

5. Saitoh TS, Fujino T. Advanced energy-efficient house (HARBEMAN house) with solar thermal, photovoltaic and sky radiation energies (experimental results). *Sol Energy*. 2001;70:63-77.

6. Kornfield J, Susskind J. On the effect of surface emissivity on temperature retrievals. *Mon Weather Rev*. 1977;105:1605-1608.

7. Becker F. The impact of spectral emissivity on the measurement of land surface temperature from a satellite. *Int J Remote Sens*. 1987;8:1509-1522.

8. Van de Griend AA, Owe M, Groen M, Stoll MP. Measurement and spatial variation of thermal infrared surface emissivity in a savanna environment. *Water Resour Res*. 1991;27:371-379.

9. Ångström AK. *A Study of the Radiation of the Atmosphere: Based Upon Observations of the Nocturnal Radiation during Expeditions to Algeria and to California*. 65. Washington, DC: Smithsonian Institution; 1915.

10. Herez A, Ramadan M, Khaled M. Review on solar cooker systems: economic and environmental study for different Lebanese scenarios. *Renew Sustain Energ Rev*. 2018;81:421-432.

11. Soria-Verdugo A. Experimental analysis and simulation of the performance of a box-type solar cooker. *Energ Sustain Dev*. 2015;29:65-71.

12. Nkhonjera L, Bello-Ochende T, John G, King'ondu CK. A review of thermal energy storage designs, heat storage materials and cooking performance of solar cookers with heat storage. *Renew Sustain Energ Rev*. 2017;75:157-167.

13. Panwar NL, Kaushik SC, Kothari S. State of the art of solar cooking: an overview. *Renew Sustain Energ Rev*. 2012;16(6):3776-3785.

14. Pohekar SD, Kumar D, Ramachandran M. Dissemination of cooking energy alternatives in India—a review. *Renew Sustain Energ Rev*. 2005;9(4):379-393.

15. Saxena A, Pandey SP, Srivastav G. A thermodynamic review on solar box type cookers. *Renew Sustain Energ Rev*. 2011;15(6):3301-3318.

16. Wentzel M, Pouris A. The development impact of solar cookers: a review of solar cooking impact research in South Africa. *Energ Policy*. 2007;35(3):1909-1919.

17. Mullick SC, Kandpal TC, Saxena AK. Thermal test procedure for box-type solar cookers. *Sol Energy*. 1987;39:353-360.

18. Li M, Jiang Y, Coimbra CF. On the determination of atmospheric longwave irradiance under all-sky conditions. *Sol Energy*. 2017;144:40-48. 201

19. Cole RJ. The longwave radiative environment around buildings. *Build Environ*. 1976;11:3-13.

20. Tang R, Etzion Y, Meir IA. Estimates of clear night sky emissivity in the Negev Highlands, Israel. *Energy Convers Manag*. 2004;45:1831-1843.

21. Fang XD. Study on saturation water-vapor pressure equations for calculation of aircraft air-conditioning systems. *J Aerospace Power*. 1995;10:329-300.

22. Berger X, Buriot D, Garnier F. About the equivalent radiative temperature for clear skies. *Sol Energy*. 1984;32:725-733.

23. Alduchov OA, Eskridge RE. Improved magnus form approximation of saturation vapor pressure. *J Appl Meteorol*. 1996;35:601-609.

24. Lawrence MG. The relationship between relative humidity and the dew point temperature in moist air: a simple conversion and applications. *Bull Am Meteorol Soc*. 2005;86:225-233.

25. Daniel OH. Digital computer reduction of AN/GMD-2 rawinsonde data. *Bulletin of the American Meteorological Society*. 43. Boston, MA: Amer Meteorological Soc; 1962:315.

26. Viswanadham Y, Ramanadham R. Studies on night radiation at some Indian Stations. *Pure Appl Geophys.* 1967;68:214-228.

27. Centeno M. New formulae for the equivalent night sky emissivity. *Sol Energy.* 1982;28:489-498.

28. Brunt D. Notes on radiation in the atmosphere I. *Q J Royal Meteorol Soc.* 1932;58:389-420.

29. Elsasser WM. Heat transfer by infrared radiation in the atmosphere. *Harvard Meteor Stud.* 1942;6:107.

30. Anderson ER. Energy Budget Studies, Water-loss Investigations, Lake Hefner Studies. Reston, VA: US Geological Survey; 1954; 71-119. Prof. paper no. 269.

31. Kondrat'ev KY. *Radiation in the Atmosphere.* New York, NY: Academic Press; 1969:915.

32. Staley DO, Jurica GM. Effective atmospheric emissivity under clear skies. *J Appl Meteorol.* 1972;11:349-356.

33. Niemelä S, Räisänen P, Savijärvi H. Comparison of surface radiative flux parameterizations: part I: longwave radiation. *Atmos Res.* 2001;58:1-18.

34. Clark G and Allen C. The estimation of atmospheric radiation for clear and cloudy skies. Proceedings 2nd National Passive Solar Conference (AS/ISES); 675-678; 1978.

35. Berdahl P, Martin M. Emissivity of clear skies. *Sol Energy.* 1984;32:663-664.

36. Swinbank WC. Long-wave radiation from clear skies. *Q J Royal Meteorol Soc.* 1963;89:339-348.

37. Sloan R, Shaw JH, Williams D. Thermal radiation from the atmosphere. *J Opt Soc Am.* 1956;46:543-547.

38. Idso SB, Jackson RD. Thermal radiation from the atmosphere. *J Geophys Res.* 1969;74:5397-5403.

39. Carmona F, Rivas R, Caselles V. Estimation of daytime downward longwave radiation under clear and cloudy skies conditions over a sub-humid region. *Theor Appl Climatol.* 2014;115:281-295.

40. Brutsaert W. On a derivable formula for long-wave radiation from clear skies. *Water Resour Res.* 1975;11:742-744.

41. Satterlund DR. An improved equation for estimating long-wave radiation from the atmosphere. *Water Resour Res.* 1979;15:1649-1650.

42. Idso SB. A set of equations for full spectrum and 8- to 14-μm and 10.5- to 12.5-μm thermal radiation from cloudless skies. *Water Resour Res.* 1981;17:295-304.

43. Prata AJ. A new long-wave formula for estimating downward clear-sky radiation at the surface. *Q J Royal Meteorol Soc.* 1996;122:1127-1151.

44. Dilley AC, O'Brien DM. Estimating downward clear sky long-wave irradiance at the surface from screen temperature and precipitable water. *Q J Royal Meteorol Soc.* 1998;124:1391-1401.

45. Crawford TM, Duchon CE. An improved parameterization for estimating effective atmospheric emissivity for use in calculating daytime down welling longwave radiation. *J Appl Meteorol.* 1999;38:474-480.

46. Iziomon MG, Mayer H, Matzarakis A. Downward atmospheric longwave irradiance under clear and cloudy skies: measurement and parameterization. *J Atmospheric Sol-Terr Phys.* 2003;65:1107-1116.

47. Raman PK. Heat radiation from the atmosphere at night. Proceedings of Indian Academy of Sciences, April 20, Indian Academy of Sciences, Bangalore; Vol 1; 815; 1935.

48. Chen B, Clark D, Maloney J, Mei W, Kasher J. Measurement of night sky emissivity in determining radiant cooling from cool storage roofs and roof ponds. Proceedings of the 20th National Passive Solar Conference, September 1; Vol. 20; 1995; Minneapolis, MN; 310–313.

49. Chourasia BK. *Heat Transfer Studies on Box Type Solar Cookers for Thermal Testing and Standardization* [Doctoral dissertation]. Delhi: IIT Delhi; 2009.

50. Duffie JA, Beckman W. *Solar Energy Processes.* 2nd. New York: Wiley; 1991.

51. Khan SY. *Thermal Performance Evaluation of Solar Box Cookers* [Doctoral dissertation]. Delhi: IIT Delhi; 2004.

52. Hollands KGT, Unny TE, Raithby GD, Konicek L. Free convective heat transfer across inclined air layers. *J Heat Trans.* 1976;98(2):189-193.

53. Kumar S, Mullick SC. Wind heat transfer coefficient in solar collectors in outdoor conditions. *Sol Energy.* 2010;84(6):956-963.